Chapter 2

Apparatus and errors.

The apparatus used for the experiments reported in this thesis is described in §2.1, while §2.2 deals with the errors in the measurements.

A general apparatus description is given in §2.1.1, while §§2.1.2 and 2.1.3 describe the methods used to make velocity measurements. The details of the temperature measurements are given in §§2.1.4 and 2.1.5.

The errors arising from measurements of the convection chamber dimensions, the rotation rate and the temperature control of the apparatus are given in §§2.2.1, 2.2.2, and 2.2.3. Errors in velocity measurements are covered in §§2.2.4 and 2.2.5; and in heat transport and temperature measurements in §§2.2.6 and 2.2.7. The final section estimates the errors in various derived quantites used in this thesis (§2.2.8).

2.1 Description of apparatus.

2.1.1 General description of the apparatus.

The apparatus consisted of two co-axial cylinders arranged so as to form an annular convection chamber, which was placed on a rotating turntable. The radii of the cylinders are denoted a and b, where $a = 25\ mm$ and $b = 80\ mm$. The convection chamber was placed so that its central axis of symmetry coincided

with the axis of rotation of the turntable. The turntable could be rotated with uniform angular velocity, Ω, where $0.0 \leq \Omega \lesssim 5.0\ rad.sec^{-1}$. Fluid filled the cavity between these cylinders and a thermally insulating base and lid made of perspex. The lid was always flat and horizontal, while different bases were used for the various measurements described in later chapters. The bases used are described below. A schematic diagram of the annulus is shown in *Figure 2.1.* The lid was in contact with the fluid at all times.

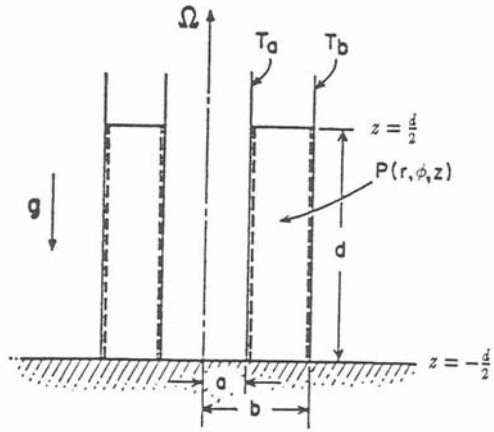

Figure 2.1: Schematic diagram of the fluid annulus. (r, ϕ, z) are cylindrical polar coordinates of a general point P, fixed in a frame moving with the apparatus which rotates uniformly at $\Omega\ rad.sec^{-1}$. The liquid occupies a region $a < r < b$ and $-\frac{d}{2} < z < \frac{d}{2}$, at $z = \frac{d}{2}$ the upper surface of the liquid is in contact with a rigid lid. From *Fowlis and Hide (1965).*

The side walls of the annulus were 2mm thick, the inner cylinder was copper, and the outer cylinder brass. They were heated (or cooled) to different constant temperatures, T_a (the inner cylinder at $r = a$) and T_b (the outer cylinder at $r = b$).

Thus a radial temperature difference $\Delta T \equiv T_b - T_a$ was applied to the fluid. For the experiments described in this thesis the outer wall was always heated and the inner cooled, so that $T_b > T_a$. The choice of the sense of ΔT was essentially arbitrary, but it seemed sensible to work with one sense of ΔT before considering the effect of reversing it. Once the wall temperatures had been established the annulus was rotated anticlockwise (looking from above), at uniform Ω. Thus the senses of Ω and ΔT correspond to those of the northern hemisphere.

Radius of inner cylinder	a	2.5	cm
Radius of outer cylinder	b	8.0	cm
Mean depth of annular cavity	$\bar{d}$	10.6–14.0	cm
Angular velocity	Ω	0.0–5.0	$rad.sec^{-1}$
Mean fluid temperature	$\bar{T}$	20	$°C$
Applied temperature difference	ΔT	4 or 10	$°C$
Kinematic viscosity of fluid	ν	1.79–1.83×10^{-2}	$cm^2.sec^{-1}$
Specific heat capacity of fluid	C_p	3.84–3.85	$J.g^{-1}.°C^{-1}$
Mean density of fluid	$\bar{\rho}$	1.045–1.088	$g.cm^{-3}$
Expansion coefficient of fluid	α	3.03×10^{-4}	$°C^{-1}$
Thermal conductivity of fluid	k	5.18×10^{-3} *	$W.cm^{-1}.°C^{-1}$

* Corrected from the March 1992 version by the author.

TABLE 2.1: Range of experimental parameters.

The temperature of the side walls was controlled by pumping water of the desired temperature through spiral channels covering the surface away from the fluid, at a rate of ~ 3.0 $litres.min^{-1}$. The water temperature was crudely controlled by a heater and fridge unit, with a proportional temperature controller attached to a low power heater providing the fine adjustment. One such system was used for each of the walls. The temperature was measured using thermocouples embedded in the walls of the annulus and in the inlet and outlet water supply tubes to the channels. There were six themocouples arranged in a vertical line in the inner wall, and 12 in a spiral around the outer wall. The supply of water to the inner and outer walls was designed to attempt to minimise the vertical

temperature gradient on each of the walls.

A list of basic fluid properties and other experimental parameters is given in *Table 2.1.*

The experiments reported in this thesis involved seven different physical boundaries to the convection chamber.

1. A fully blocking thermally insulating barrier, which was a 2.5 mm thick sheet of perspex, and blocked the entire radius and height of the annulus at $\phi = \pm\pi$.

2. A fully blocking thermally conducting radial barrier which was a sheet of copper 0.47 mm thick and blocked the entire radius and height of the annulus at $\phi = \pm\pi$. The barrier was insulated around its edges by a 0.94 mm thick plastic surround to prevent conduction from the outer wall to the inner wall radially through it.

3. A system with variable depth, $d = d(\phi)$, which combined a fully insulating radial barrier with a sloping base so that the depth was a linear function of ϕ.

4. A system with variable depth, $d = d(r, \phi)$, which combined a fully blocking thermally insulating radial barrier with a sloping base which made the depth a linear function of both r and ϕ.

5. A partially blocking barrier with a height of $\frac{2}{3}d$, and an angular width of 30°, which rested on the bottom of the annulus and occupied the region

$$a < r < b, \quad \pi - \frac{\pi}{12} < \phi < -\pi + \frac{\pi}{12}, \quad -\frac{d}{2} < z < \frac{1}{6}d.$$

6. A partially blocking barrier with a height of $\frac{2}{3}d$, and an angular width of

60°, which rested on the bottom of the annulus and occupied the region

$$a < r < b, \quad \pi - \frac{\pi}{6} < \phi < -\pi + \frac{\pi}{6}, \quad -\frac{d}{2} < z < \frac{1}{6}d.$$

7. A partially blocking barrier with a height of $\frac{1}{3}d$, which rested on the bottom of the annulus, with the same dimensions as the $\frac{2}{3}d$, 30° wide barrier, except it had half the height. This barrier was quite similar to the 'type C' topography used by *Leach (1975)*, which was a one-third barrier occupying the entire radial width of his annulus (which had different dimensions) but was rather shorter in ϕ having an angular width of about $\pi/15$.

Figure 2.2 shows schematic diagrams which illustrate the main annulus configurations described above, which the reader may find useful to refer to at later stages in this thesis.

2.1.2 Velocity measurements.

Fluid motions were visualized by a technique involving neutrally buoyant tracer particles. Historically this technique was developed by *Douglas, Hide and Mason (1972)* and *Jonas and Kent (1979)*. The present velocity measurement system was developed by *Jackson and Hignett (1984)*, *Bell (1984)* and *Bell and Jackson (1985)*.

A schematic cross-section of the velocity measurement annulus is shown in *Figure 2.3*.

The fluid motions within the annulus were observed by means of the Video Velocity Acquisition System (VVAS). A diagram of VVAS is shown in *Figure 2.4*. Flow within the annulus cavity was visualized by means of small neutrally buoyant polystyrene beads of diameter $601 - 709\mu m$. The fluid used was a water-glycerol mixture with a density of $\rho \approx 1.05 - 1.09\ g.cm^{-3}$ at $20°C$. A few drops of commercial fungicide were added to the fluid to discourage the fungal growths to

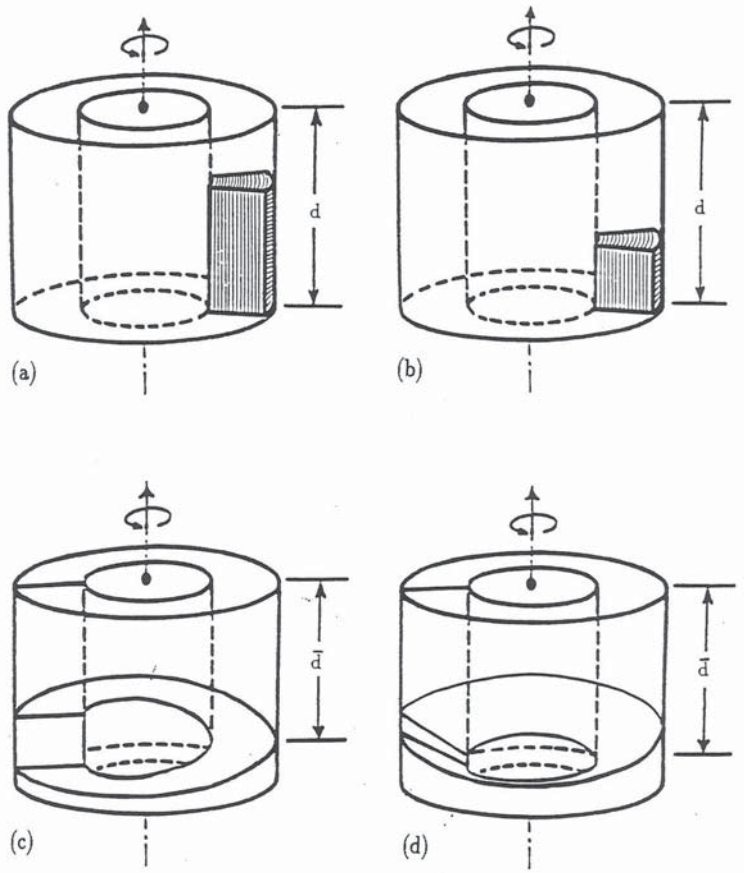

Figure 2.2: Diagram depicting several of the annulus configurations mentioned in the text. *(a)* Two-thirds partial barrier (5), *(b)* one-third partial barrier (7). *(c)* Sloping base system with $d = d(\phi)$ (3), the full radial barrier is situated opposite $\phi = 0$ so that $d(\pi) = 90\ mm$, $d(-\pi) = 128\ mm$, and the mean depth $\bar{d} = 109\ mm$. *(d)* Sloping base system with $d = d(r, \phi)$ (4), with depths $d(b, \pi) = 89\ mm$, $d(a, \pi) = 114\ mm$, $d(b, -\pi) = 102\ mm$, $d(a, -\pi) = 127\ mm$; $\bar{d} = 106\ mm$.

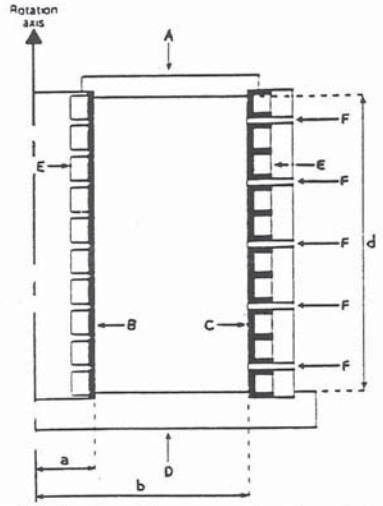

Figure 2.3: A schematic cross-section through the velocity measurement annulus. The labelled features are: A, insulating lid; B, inner cylinder; C, outer cylinder; D, insulating base; E, water channels; F, transparent acrylic inserts at heights $z = 16\ mm$, $43\ mm$, $70\ mm$, $97\ mm$, and $124\ mm$. The radii of the inner and outer walls were a and b respectively, while the annulus cavity was of depth d. From *Hignett et al. (1985).*

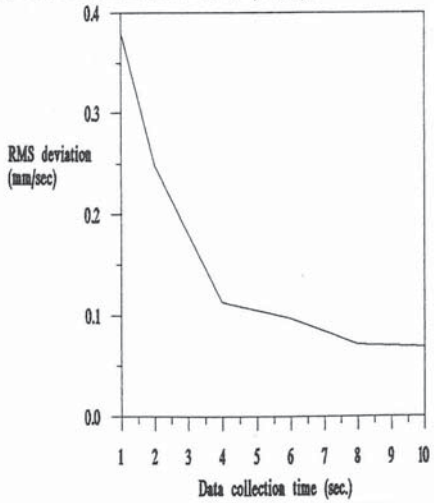

Figure 2.5: Measurements of root mean square deviations in velocity from 0 $mm.sec^{-1}$ plotted against data collection time, for velocity data taken by VVAS (see text). Results of *Jackson and Hignett (1984).*

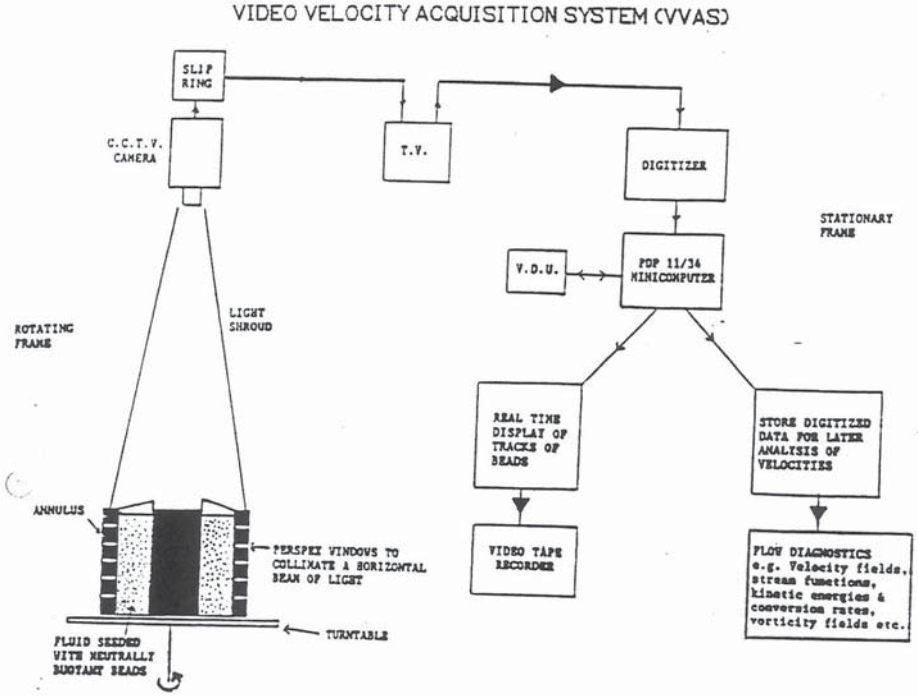

Figure 2.4: Diagram of the Video Velocity Acquisition System (V.V.A.S.). The annulus is shown seeded with neutrally buoyant particles which act as tracers for the fluid within it. The fluid can be illuminated by a horizontal beam of light at one of five different levels. The camera can observe the horizontal velocities of the tracers at one of the levels. The image can then be digitized and stored on disk for later analysis. Diagram provided by D. Johnson (private communication).

which water–glycerol solutions are susceptible. For this mixture the beads spread over the depth of fluid within the cavity. The lid of the annulus was made of clear thermally insulating perspex and when the cavity was illuminated by a horizontal sheet of light the beads showed as tiny bright specks. As *Figure 2.3* shows the fluid could be illuminated by a sheet of light at one of five vertically displaced levels. At any one of these levels the motion of these beads in the horizontal plane could be observed by a camera mounted above the annulus. Information about how the flow changed with height could be inferred by looking at the horizontal motions at different light levels, giving information about the three-dimensional structure of the flow. However the measurement technique did not allow the determination of vertical velocities from the continuity equation (1.2), as these were not measured directly and the errors in the velocity measurements did not allow them to be inferred from the horizontal motions.

The problem with attempting to infer the vertical velocities from equation (1.2) can be illustrated as follows. If horizontal velocities can be determined to an accuracy of 0.09 $mm.sec^{-1}$ (see §2.2.4), then the errors produced by inferring the vertical velocities by the incompressibility condition (equation (1.2)) can be estimated as follows. Using *Batchelor (1967)*, p602, equation (1.2) in cylindrical polar coordinates is

$$\frac{1}{r}\frac{\partial(ru)}{\partial r}+\frac{1}{r}\frac{\partial v}{\partial \phi}+\frac{\partial w}{\partial z}=0,$$

so that

$$w=-\int_{z_1}^{z_2}\left(\frac{1}{r}\frac{\partial(ru)}{\partial r}+\frac{1}{r}\frac{\partial v}{\partial \phi}\right)dz.$$

Now let (u_e, v_e, w_e) be the errors in (u, v, w), so that

$$w+w_e=-\int\left(\frac{1}{r}\frac{\partial}{\partial r}[r(u+u_e)]+\frac{1}{r}\frac{\partial}{\partial \phi}(v+v_e)\right)dz.$$

Hence

$$|w_e|\sim\frac{\Delta u_e\Delta z}{\Delta r}+\frac{\Delta v_e\Delta z}{\bar{r}\Delta\phi}.$$

Using $\Delta u_e=\Delta v_e\sim 0.9\times10^{-4}\ m.sec^{-1}$, $\Delta r=(b-a)$, $\bar{r}=(a+b)/2$, $\Delta\phi=2\pi\bar{r}$, and $\Delta z=3\times10^{-2}\ m$ (the height difference between two light levels), then $w_e\sim10^{-4}\ m.sec^{-1}$, is the error in calculating w.

Next it is possible to estimate the magnitude of w from the effect of Ekman pumping (since rotational effects tend to make $\partial w/\partial z\sim 0$), see e.g. *Holton (1979)*, $w_{ek}=\zeta_g\delta_{ek}/2\pi$. Where the vertical component of the relative geostrophic vorticity, $\zeta_g\approx\partial v_g/\partial r$ (where v_g is the ϕ component of the geostrophic velocity) since the forcing is assumed axisymmetric so that $\partial/\partial\phi\approx 0$. Then if $v_g\sim 5\times10^{-3}\ m.sec^{-1}$, and $\delta_{ek}\sim10^{-3}\ m$, then $w_{ek}\sim2\times10^{-5}\ m.sec^{-1}$. This figure agrees very closely with the estimation of vertical velocities at 0.01 $mm.sec^{-1}$ by *Jackson and Hignett (1984)*. Since $|w|\sim|w_{ek}|\ll|w_e|$ there is no prospect of calculating w between the velocity measurement levels using the incompressibility condition. However *Read (1989)* has suggested that w might be calculated by using the quasi–geostrophic thermodynamic equation. He used certain simplifications to calculate w for a regular wave flow, but states that a more general expression for w could also be derived. For further details see *Read (1989)*.

The beams of light were $2mm$ deep by the outer wall, spreading to $4mm$ by the inner wall, the light entered the cavity through the five acrylic inserts mentioned in *Figure 2.3*.

The camera was mounted on the annulus turntable directly above the annulus so that it observed the flow in the rotating frame of the annulus, and connected to the remainder of VVAS via an electrical slip ring. The flow within the annulus could either be observed directly on a T.V. screen or else it could be digitised. The digitised camera image was then fed to a PDP 11/34 minicomputer, from there it was either stored on disk for later analysis, or else observed in real time

as particle trajectories on the T.V.screen. The T.V. output could be recorded by a video tape recorder if desired. The video recorder proved most useful for observing slowly evolving flows as it enabled a long period of observation to be recorded and to be played back up to 72 times faster.

2.1.3 Procedure for making velocity measurements.

Sets (or runs) of velocity data were taken by first setting ΔT and Ω, then waiting for the flow to settle down and finally recording velocity data using VVAS.

When the apparatus was turned on, it took some time for the applied ΔT to settle across the cavity. Once the temperature controllers indicated that the water being pumped around the inner and outer cylinders had reached the desired temperatures a certain time was let elapse so that ΔT could become established across the cavity. Measurements of the temperatures indicated that this whole process took around two and a half to three hours, consequently this length of time was always allowed to elapse before any data was taken. As the temperature control of the apparatus was usually left on overnight, this meant that for the large majority of runs ΔT had been established either the previous day, or several days beforehand and left unaltered in the meantime. Any small corrections to ΔT, of the order of less than 1 K, were found to become established much more rapidly, and a period of 45 minutes allowed for these to settle. Chart recorder measurements of the temperature of a ring thermocouple showed that this was adequate time for the flow to settle down.

The temperature measurement scans were usually taken over 10 minutes, and their mean and standard deviations calculated.

The rotation rate was set at least 45 minutes before data was taken for a given run, thus allowing the motions in the fluid to settle down and spin-up effects to die away. Though this time was about the minimum acceptable (from experience

this was about twice the time taken by the flow to reach its final state, which also agrees quite closely with theoretical estimates of the spin-up time for the fluid, see below), it was required for measurements at very low angular velocities (around a few tenths of a $rad.sec^{-1}$) because the fluid velocities within the annulus were often very small (of the order of 0.1 $mm.sec^{-1}$), so that unless the tracer beads were perfectly neutrally buoyant they would either gradually settle to the bottom or float to the top of the cavity. At higher Ω the onset of waves tended to relieve this problem, as they mixed the fluid.

The time taken for the fluid to feel the effect of rotation, starting from a state of rest can be estimated following *Greenspan (1968)*. Greenspan describes the physical processes of spin–up as follows: boundary layers are seen to form on horizontal surfaces within the first few revolutions following the impulsive start of rotations. Non–rotating fluid is sucked into these layers, spun–up by viscous action, and returned to the interior at the vertical side wall.

Using equation (1.6), to estimate the viscous action, $|\partial u/\partial t| \sim |\nu \nabla^2 u|$, so that scaling gives a characteristic time–scale as, $t \sim L^2/\nu$, where L is a typical length scale. Since viscous action is felt in the Ekman boundary layers (see above) the appropriate length scale is that of the Ekman boundary layer thickness, thus $L \sim \delta_{ek} = \sqrt{\nu/\Omega}$ (*Tritton (1988)*), and $t \sim 1/\Omega$. Barring a factor of 2π this is the rotation period of the annulus. The next stage is that vertical velocities induced by the Ekman layers penetrate the interior of the fluid. Thus $w = \zeta \delta_{ek}/2\pi$ (see e.g. *Holton (1979)*). Where ζ is the vertical component of the relative vorticity and δ_{ek} is the thickness of the Ekman layer. It must be stressed that in this case ζ may not be the geostrophic vorticity, as the fluid has not yet achieved steady–state, and so $\partial \vec{u}/\partial t$ in equation (1.6) cannot necessarily be neglected, and possibly other terms may also be important. The calculation of w_{ek} above yields a different result because the geostrophic vorticity is used. If the flow is assumed to

be axisymmetric, so that $\partial/\partial\phi \approx 0$, then $\zeta \approx \partial v/\partial r$. δv is estimated as the solid–body velocity, Ωr, since the interior fluid gets 'left behind' when the walls, lid and base start to rotate. Thus, using $\Omega = 1\ rad.sec^{-1}$, and $w \sim 1 \times 10^{-4}\ m.sec^{-1}$, the time taken for the spun–up fluid to traverse a distance d at speed w is $d/w \approx 20$ minutes. Thus the characteristic spin–up time for the annulus is $\sim$ 20 minutes, which agrees quite closely with experience (see above).

A run of velocity data normally consisted of 25 scans, each scan being a view of a given level in the fluid over a period of a few seconds, with an interval between each scan. The scans were taken by cycling through the five light levels in turn, and usually five scans were taken of each level.

The VVAS data consisted of velocities randomly distributed over the field of view. These were analysed using a least squares fitting routine which fitted basis functions to the velocity data points, enabling the velocity field to be reconstructed on an evenly spaced grid. The basis functions used by the least squares fitting routine are given below:

$$\sum_k \sum_m \left\{ a_{k,m} \sqrt{\frac{b}{r}} \sin(m\pi x) \cos(k\phi) + b_{k,m} \sqrt{\frac{b}{r}} \sin(m\pi x) \sin(k\phi) \right\}.$$

Where ϕ is the azimuthal coordinate, and x is the scaled radius, $x = (r - a)/(b - a)$. The functions were fitted using a radial wavenumber $1 \leq m \leq 6$, and an azimuthal wavenumber $1 \leq k \leq 16$. The least squares fitting routine is described in some detail in *Jackson and Hignett (1984)*, *Bell (1984)* and *Bell and Jackson (1985)*.

2.1.4 Temperature and heat transport measurements.

Fluid temperature measurements were made by using thermocouples, while simultaneous measurements were made of the total heat transported through the inner side wall, which was used to calculate the fluid heat transport.

The outer cylindrical wall of the annulus consisted of two sections placed one on top of the other with an acrylic insert between them which supported an array of 32 equally spaced (over ϕ) thermocouples. The thermocouples were arranged so as to measure temperatures at mid-radius ($r = \bar{r}$) in the cavity, at a height 7.0 cm below the lid ($z = 0$). They were constructed of copper-constantan junctions having a sensitivity of approximately 40 $\mu V.K^{-1}$. The thermocouples were made of enamelled wires, and the soldered junctions varnished, to help insulate the thermocouples from the fluid and to prevent any stray e.m.f.'s that could be caused by electrochemical effects. The thermocouple ring provided data on the way fluid temperatures varied with Ω in the form of a temporal mean. For the experiments which included some kind of barrier a temperature drop across the barrier was usually observed which was defined as,

$$\Delta T_B \equiv T^{warm} - T^{cool} \tag{2.1}$$

where T^{warm} was the temperature of the warmest thermocouple in the ring at any given Ω and T^{cool} the temperature of the coolest ring thermocouple.

The heat transport measurements were inferred from the temperature rise and flow rate of the cooling fluid circulating through the inner cylinder. The temperature difference being measured by a thermopile constructed from 25 copper-constantan junctions, which produced its output, θ in μV. The flow rate F was measured by a Pelton–wheel flow meter and held constant to within 0.5%. The output from the thermopile was highly sensitive to external conditions, for this reason the annulus was kept in an enclosure which was temperature controlled to $\pm 0.2^0 C$ while the laboratory was kept at a constant temperature of $22 \pm 2^0 C$. Even so it was necessary to perform a series of null measurements over the range of Ω to be used before and after each set of experiments. The null experiments are described in §2.1.5, and the null output is denoted N (μV). The total fluid heat transport (H_{total}) to the inner cylinder was therefore calculated as

$$H_{total}(watts) = \frac{[\text{thermopile o/p} - \text{null}](\mu V) \times \text{flow rate}(Hz)}{\text{flow meter calibration constant}(\mu V.J^{-1})}. \quad (2.2)$$

Using the equation above to define the symbols below, this is represented as

$$H_{total} = \frac{(\theta - N)F}{K}. \quad (2.3)$$

To calculate Nu (see equation (1.17)), it is necessary to calculate H_{cond} for the fluid. The conductive heat flux vector was $\vec{H}_{cond}(W.m^{-2}) = -k\nabla T$. In the case of the differentially heated annulus ΔT was applied radially, so that this can be reduced to $H_{cond}(watts) = -k(2\pi rd)\partial T/\partial r$. Separation and integration between a and b for r and T_a and T_b for T then yields

$$H_{cond} = \frac{2\pi k \Delta T d}{\ln(b/a)}. \quad (2.4)$$

Further details about the apparatus may be found in *Hignett et al. (1985)*, and in detail in *Small (1989)*.

It is to be expected that the thermocouple ring had some effect on the fluid motions, despite efforts to keep the thermocouples and junctions as small as reasonably possible. This problem has been discussed in some detail by *James, Jonas and Farnell (1981)*, and by *Hignett et al. (1985)*. They concluded that the thermocouple ring does not change the basic character of the flow.

2.1.5 Procedure for making temperature measurements.

The collection of data was done in three distinct stages; (*i*) initial series of null measurements, (*ii*) heat transport and temperature measurements, and (*iii*) final series of null measurements.

(i) Initial null measurements: the annulus cavity was drained of fluid and washed with deionized water and drained several times, before being dryed out completely with a hot air blower. This was done to prevent any build up of

glycerol deposits in the annulus cavity. It was also important to ensure that no water was left in the cavity which could transport heat by its latent heats of vaporization and condensation.

When the cavity was clean and dry a polystyrene insert, shaped to allow for the thermocouple ring, was placed in the cavity to prevent transport of heat by air currents, and to further insulate the cavity. After this the temperature difference ΔT was applied, and a series of measurements of θ (in μV) made over a range of Ω from $0.0 - 5.0$ $rad.sec^{-1}$ inclusive at intervals of 0.5 $rad.sec^{-1}$. Each time the desired Ω was selected and then the heat transport was monitored using a chart recorder until it had settled down. After this a set of 150 measurements at 4 *sec* intervals were taken of each of the thermopile output, wall temperatures, flow rates and various other experimental parameters. This was done automatically and the means and standard deviations of the data calculated. The mean values of the null measurements, $N = N(\Omega)$ in μV were then subtracted from the thermopile measurements made in the presence of the fluid (see equations (2.2), (2.3)) so as to allow for the effect of the apparatus and environment on the heat transport measurements.

(ii) Heat transport and temperature measurements: Next the polystyrene insert was removed, the annulus cavity filled with water-glycerol solution and the lid put on, taking care to ensure that there were no bubbles underneath it. The fluid was previously de-gassed by being vacuum pumped for a day or so. Any bubbles that later formed were removed from the walls of the cavity and the thermocouple ring using a fine brush.

With the appropriate ΔT applied the annulus was rotated at uniform Ω until the flow had settled down. This was seen by means of the chart recorder which monitored θ and one of the ring thermocouples. When the flow had settled down, usually 241 measurements at 5 *sec* intervals were taken of θ, each of the

ring thermocouples and of the various other experimental parameters required for the calorimetry and accurate measurement of the wall temperatures. In this way a large range of Ω was covered. For measurements at Ω intermediate between the 0.5 $rad.sec^{-1}$ intervals at which null measurements were made the values of the null measurements were estimated by linear interpolation.

(iii) Final null measurements: these repeated the initial null measurements. They were performed to check that the behaviour of the apparatus after the experiments was consistent with its behaviour before and also to estimate the accuracy of the results (see §2.2.6).

2.2 Errors in the measurements.

The following sources of errors are considered: (§2.2.1) variations in the dimensions of the annulus cavity, and Ω (§2.2.2). §2.2.3, errors in ΔT; velocity measurement errors arising from measurements of bead velocities (§2.2.4), and errors arising from fitting the velocity field (§2.2.5).

Errors in the heat transport measurements are considered in §2.2.6, and in the thermocouple ring measurements in §2.2.7. Finally in §2.2.8 errors in quantities derived from the experimental data are estimated.

2.2.1 Errors in the cavity dimensions.

The errors in the dimensions of the annulus were considered as follows. Sixteen measurements were taken of the radius of the inner cylinder, giving the value $a = 25.00\ mm$ with a standard error of $a_E = 0.04\ mm$. The radius of the outer cylinder was assumed to be accurate to the design specification of $b = 80.0\ mm$, and based on the value of a_E a somewhat cautious value of $b_E = 0.1\ mm$ was assumed. The error in d was assumed to be $d_E = 0.5\ mm$. Hence the fractional errors a_σ, b_σ and d_σ were calculated as

$$a_\sigma = \frac{a_E}{a}\ ,\ b_\sigma = \frac{b_E}{b}\ ,\ d_\sigma = \frac{d_E}{d}. \tag{2.5}$$

Thus $a_\sigma = 0.16\%$, and $b_\sigma = 0.13\%$.

2.2.2 Errors in rotational control.

The rotation rate of the annulus was measured before and after each experiment by means of an optically activated timer. Usually the mean of ten rotation periods was used to caculate Ω. The optically activated timer was assumed to be correct to the manufacturers specification of 0.0003%, this was considered to be so small compared with other errors that it could safely be neglected.

Previous tests had shown the rotational stability of the annulus to be about 1 part in 20,000 (0.005%), though in the worst case over a period of about 12 minutes the stability was seen to be 1 part in 1,500 (0.07%). Thus the fractional error in Ω, $\Omega_\sigma = 0.07\%$. Although this was only a tiny fraction of 1% and was possibly negligible compared with other errors discussed below the error in Ω was included in the calculations for completeness.

2.2.3 Errors in temperature control.

During the course of the experiments repeated measurements were taken of the inner and outer wall temperatures at various heights. From these the mean temperature difference ΔT was calculated and its standard deviation ΔT_{SD}. The standard deviation used was the largest out of the set of runs comprising the experiment, or null measurements. The standard error in ΔT, ΔT_* was calculated as $\Delta T_* = \Delta T_{SD}/\sqrt{N}$ where N was the number of measurements taken of ΔT, usually 241 for the heat measurement experiments, or 150 for the null experiments.

There were also observed to be vertical variations in the wall temperatures,

which would not have been important in terms of the repeatability of the measurements provided that they held a constant value as say a percentage of ΔT. However they varied by a few percent during each experiment. The variability this caused in the wall temperatures for each of the walls individually may be expressed as

$$T_V = \frac{\text{vertical variation}(\%)}{100\sqrt{N}} \times \Delta T$$

where the superscript *'in'* or *'out'* applied to T_V will denote a reference to the inner or outer wall. Then the total standard error in the measurement of ΔT due to T_V was $\Delta T_V = \sqrt{(T_V^{in})^2 + (T_V^{out})^2}$, and the standard error in ΔT, ΔT_E was

$$\Delta T_E = \sqrt{\Delta T_*^2 + \Delta T_V^2}. \tag{2.6}$$

The fractional error in ΔT, ΔT_σ was then calculated as

$$\Delta T_\sigma = \frac{\Delta T_E}{\Delta T}. \tag{2.7}$$

2.2.4 Errors in bead velocity measurements.

This section and §2.2.5 are concerned with the errors involved with the fitted velocity fields produced by VVAS (§2.1.2, Figures 2.3, 2.4).

This problem is discussed in detail in *Jackson and Hignett (1984)*, *Bell (1984)* and *Bell and Jackson (1985)*. The treatment here summarises their conclusions.

The performance of VVAS can be assessed in two separate parts; *(i)* consideration of how closely the measurements of bead velocities correspond to the horizontal components of fluid motion, and *(ii)* to what extent the fitted field represents the measurements of the bead velocities. *(i)* is discussed in this section, and *(ii)* in §2.2.5.

Jackson and Hignett (1984) attempted to determine the accuracy of measurement of bead velocities by considering *(a)* random errors associated with the velocity measurements of individual particles, and *(b)* the systematic calibration errors associated with the system.

(a) The annulus was kept stationary whilst filled with fluid and beads. Measurements of root mean square (RMS) deviations from the expected velocities of 0 $mm.sec^{-1}$ were recorded against the data collection time. *Figure 2.5* shows their results, they concluded that a data collection time of about four seconds was most appropriate. The main source of random errors was considered to be quantization errors of the TV and digitizing system. These were 1 part in 256 along the y-axis and 1 in 512 on the x-axis. The errors arose because the end of each velocity track was only located to the nearest box on the grid, and depended on the time taken by a bead to travel from one end to the other (the data collection time).

A further problem was that VVAS used a linear fit between end points, so that if the data collection time was too long the bead path was more likely to have significant curvature, also only the average velocity may be calculated for the track. For this reason it was desirable to keep the data collection time short.

(b) To measure systematic errors they drained the annulus and placed a plate with marker holes in it. The plate was rotated relative to the annulus at known angular velocity. As the position of the marker holes was known Jackson and Hignett were able to find that the zonal velocities were measured to within 0.5% for data collection times of four seconds or more.

Bell (1984) pointed out several other sources of error that may arise.

1. If a bead was moving down the screen, its coordinates were measured at slightly longer time intervals than a stationary bead, due to the finite time it took the camera to scan down the screen. He estimated that this could

cause an error in velocity of $\sim 0.001\ mm.sec^{-1}$.

2. If the flow was unsteady, then the data collection time must be much less than the characteristic time-scale that the flow changes over.

3. Vertical shears in the flow could cause errors due to the finite thickness of the horizontal light beams. He estimated the error thus caused to be $\sim 0.06\ mm.sec^{-1}$.

4. The voltage ramp that was used to draw the electron beam across the (x,y) grid in the camera might have been slightly non-linear. This would distort the image and so record a false position for a bead at any given time.

5. The location of the bead was marked by the transition from dark to light recorded at its left hand edge. A bead's image can be two or three times its actual diameter and this causes an inaccuracy in its recorded position. The image was larger because of sympathetic glow around an illuminated point on the camera's phosphor screen, and possibly also due to imperfections in the camera lens.

Bell and Jackson (1985) considered in addition the possibilities of VVAS mistracking a bead, *i.e.* commencing a track with one bead and ending it with another bead. Possible sources of mistracking could have been

1. The bead at the start of the track moved vertically out of the horizontal light beam, while another bead moved vertically into the beam at the end of the data collection time. VVAS would then use the second bead to end the track started by the first.

2. Unequal illumination could cause a bead near the digitization threshold to pass over it, so that the bead would either "appear" or "disappear".

3. A bead could have been obscured by another bead.

They attempted to reduce the possibility of mistracking by placing a limit on the acceptable range of track distributions. They also calculated the error in position due to temperature variations in the fluid causing variations in the refractive index of the fluid. This error was estimated to be at maximum, $0.1\ mm$.

The large number of possible sources of error make it very difficult to estimate a suitable error for the velocities. This may be a reason why previous authors have seemed reluctant to use the VVAS system to obtain quantitative measurements. For the velocity measurements with the full radial barriers, a data collection time of up to around 50 *sec* was used, because the fluid velocities were so small (and hence the bead tracks very short). From *Figure 2.5* the appropriate error in the horizontal velocities was $0.07\ mm.sec^{-1}$. Using the largest of the (quantified) errors suggested by *Bell (1984)* (no 3, above), which was $0.06\ mm.sec^{-1}$ leads to an error of $0.09\ mm.sec^{-1}$ in the horizontal velocity measurements. This error has been used for all the horizontal velocity measurements in this thesis, and generally appears to give reasonable looking error bars on the figures where velocity results have been plotted. In one or two cases there are velocity measurements which seem to be significantly different from the other results, and well beyond the error bars, these are considered to be due to one or more of the many other sources of errors, including those discussed in §2.2.5 below.

2.2.5 Errors in fitted velocity field.

This is a complex topic, as the errors depend upon the details of the flow being examined and the method of analysis used. However the fact that the maximum radial and azimuthal wave numbers fitted were 6 and 16 means that it may be immediately appreciated that fluid motions with length scales of less than $(b-a)/6 \approx 9\ mm$ in radius, and of order $\pi(a+b)/16 \approx 21\ mm$ in azimuth were

very poorly represented (21 mm corresponds to about 23^0 in ϕ). Scales larger than those should have been increasingly well represented as they increased in size. A list of other factors likely to affect the accuracy of the fitted field is given below.

- Accuracy of particle velocities.
- Concentration of particles.
- Distribution of particles.
- Analysis scheme adopted.
- Structure of flow being studied.

Due to the complexity of this aspect of the problem, this is not gone into in any further detail here, though the interested reader should refer to the sources given above in §2.2.4.

2.2.6 Errors in heat transport measurements.

Means and standard deviations were calculated for the 150 measurements of thermopile output taken at each value of Ω during the null measurements described in §§2.1.4 and 2.1.5. The thermopile output, θ (in μV), has standard deviation, θ_{SD} and standard error, θ_*, $\theta_* = \theta_{SD}/\sqrt{150}$, for each value of Ω. Let θ_{sys} be the difference in the thermopile output for the two sets of null measurements (one before and one after each set of experiments). As it was difficult to know when and how rapidly θ_{sys} arose during the set of experiments it was treated as a further 'random' error, since during any given experiment there was no way of knowing which way it was acting, if at all. So the total error in the null measurements was $\theta_B = \sqrt{(\theta_*)^2 + (\theta_{sys})^2}$.

For the heat transport results, repeated measurements of θ were taken and their means and standard deviations calculated. While the deviations in these measurements allowed for the variation in thermopile output and inner cylinder flow rate they could not allow for the errors in the null measurements, θ_B. The method of calculation of the heat transport was shown in equations (2.2) and (2.3). To consider the effect of an error in the null measurements, let there be an error θ_B in the null and let h be the resulting error in the heat transport, then

$$H_{total} + h = \frac{(\theta - N - \theta_B)F}{K},$$

so that $h = -\theta_B F/K$.

The standard deviations calculated from the measurements of heat transport H_{SD} already allow for any random error in θ and F, so the combined error in H_{total} was

$$H_B = \sqrt{h^2 + \frac{H_{SD}^2}{n}}, \tag{2.8}$$

where n is the number of measurements, with the fractional error in H, H_σ given by

$$H_\sigma = \frac{H_B}{H_{total}}. \tag{2.9}$$

The heat transport was calculated in terms of Nu, given by equation (1.17). Where H_{cond} is given by equation (2.4). Assuming that k is well known and calling the fractional error in H_{cond}, $(H_{cond})_\sigma$, then [1]

$$(H_{cond})_\sigma = \sqrt{\Delta T_\sigma^2 + d_\sigma^2 + a_\sigma^2 + b_\sigma^2}, \tag{2.10}$$

[1] Strictly speaking (2.10) should have a_σ^2 and b_σ^2 divided by $\ln^2(b/a) \approx 1.3$. Thus (2.10) slightly overestimates the error $(H_{cond})_\sigma$.

so that the fractional error in Nu, Nu_σ was

$$\mathrm{Nu}_\sigma = \sqrt{H_\sigma^2 + (H_{cond})_\sigma^2}. \tag{2.11}$$

The normalized heat transport data was calculated by dividing $\mathrm{Nu}(\Omega)$ by $\mathrm{Nu}(\Omega = 0)$. The accuracy of $\mathrm{Nu}(\Omega = 0)$ was further improved by taking more than one measurement at $\Omega = 0$. As the fractional RMS deviation in the mean values of $\mathrm{Nu}(\Omega = 0)$ was much less than the value of Nu_σ then an estimate of the fractional error in $\mathrm{Nu}(\Omega = 0)$, $\mathrm{Nu}(\Omega = 0)_\sigma$ was given by $\mathrm{Nu}(\Omega = 0)_\sigma = \mathrm{Nu}_\sigma/\sqrt{n}$, where n is the number of measurements made of $\mathrm{Nu}(\Omega = 0)$.

Thus the errors in the normalized heat transport data were

$$\left[\frac{\mathrm{Nu}}{\mathrm{Nu}(\Omega = 0)}\right]_\sigma = \sqrt{\mathrm{Nu}_\sigma^2 + \mathrm{Nu}(\Omega = 0)_\sigma^2}. \tag{2.12}$$

The largest fractional error in H_{cond} was 0.7%, so that the largest error in H_{cond} was about 0.03 *watts*. Since this was from 2.5 to 23 times smaller than the error in H_{total}, when H_{adv} was required separately from Nu, its error was assumed to be the same as that for H_{total}.

Systematic errors in each measurement from the thermopile and other experimental parameters were removed by subtracting the open circuit voltage from the measurents before they were recorded.

A possible systematic error can arise in the conducting barrier experiments (chapter 4), from radial heat conduction through the copper barrier. Attempts were made to minimize this by making the barrier very thin (0.47 *mm*) and surrounding it with plastic edging, to insulate it from the inner and outer walls of the annulus. The plastic edging was 0.94 *mm* thick. Using values for the thermal conductivities of copper and plastic of, $k_{copper} = 401\ watts.m^{-1}.K^{-1}$ and $k_{plastic} \approx 0.2\ watts.m^{-1}.K^{-1}$ gave the radial heat conduction through the barrier as 0.07 *watts* at $\Delta T = 10\ K$. Since this was much less than the errors in the heat

transport measurements, clearly the effect of radial heat conduction through the barrier can be neglected.

Since the original null measurements for runs 4U-8L, 8M-9L and 012-046 were not available the error in the null measurements for those runs was estimated from runs 126-391.

2.2.7 Errors in thermocouple ring measurements.

The standard deviations in the temperature reading for each of the 32 ring thermocouples were calculated. T^{warm} and T^{cool} were defined in equation (2.1), let the subscript 'SD' indicate the standard deviations in those quantities, then as 241 measurements were usually made during each experiment the standard errors in these quantities, T_B^{warm}, T_B^{cool} were $T_B^{warm} = T_{SD}^{warm}/\sqrt{241}$ with a similar equation for T_B^{cool}. As ΔT_B was defined in (2.1), then the error in ΔT_B, $(\Delta T_B)_B$ was given by

$$(\Delta T_B)_B = \sqrt{(T_B^{warm})^2 + (T_B^{cool})^2}. \tag{2.13}$$

A typical $(\Delta T_B)_\sigma$ was calculated by using a mid-range value for ΔT_B.

A particularly large error can be seen in ΔT_B at $\Omega = 0$, when it would be expected that $\Delta T_B = 0$. This can be accounted for by considering a systematic error in the thermocouple ring readings arising from small radial displacements of the thermocouples away from their correct position at $r = \bar{r}$. If, when $\Omega = 0$, the radial temperature gradient can be approximated by $\partial T/\partial r \approx \Delta T/(b-a)\ ^\circ C.mm^{-1}$, then the radial displacement of a thermocouple will affect its temperature by $0.07\ ^\circ C.mm^{-1}$ at $\Delta T = 4\ ^\circ C$, and $0.2\ ^\circ C.mm^{-1}$ at $\Delta T = 10\ ^\circ C$. Thus very small displacements of the thermocouples away from $r = \bar{r}$ could easily lead to systematic errors of the order observed in the measurements. When $\Omega \neq 0$ the results of *Bowden and Eden (1968)* show that $\partial T/\partial r$ becomes very small, so that

this source of error would then become virtually negligible.

2.2.8 Errors in derived quantities.

The experimental parameters and data were used to derive various non-dimensional numbers, as well as certain quantities used to analyse the results (q.v. Chapter 3). These were Θ, τ, Pr, Ra and Ek, as well as the quantities A_*^{-1}, H_η, H_ζ and H_{total}.

In general let i_B be the standard error in any quantity i, and let i_σ be the associated fractional error. Then if $i = i(x, y, z)$

$$i_B^2 = \left(\frac{\partial i}{\partial x}\right)^2 x_B^2 + \left(\frac{\partial i}{\partial y}\right)^2 y_B^2 + \left(\frac{\partial i}{\partial z}\right)^2 z_B^2$$

and $i_\sigma = i_B/i$. So that the fractional error in Θ (see equation (1.12)) was

$$\Theta_\sigma = \sqrt{\Delta T_\sigma^2 + d_\sigma^2 + 4\Omega_\sigma^2 + \frac{4(b_B^2 + a_B^2)}{(b-a)^2}}. \tag{2.14}$$

Similarly, for τ (see equation (1.13)), by assuming that ν is well known, the fractional error in τ is

$$\tau_\sigma = \sqrt{\frac{25(b_B^2 + a_B^2)}{(b-a)^2} + 4\Omega_\sigma^2 + d_\sigma^2}. \tag{2.15}$$

As Pr= ν/κ it was assumed that errors in it were negligible, following the assumptions of equations (1.1) and (1.5). The fractional error in Ra is

$$\mathrm{Ra}_\sigma = \sqrt{\Delta T_\sigma^2 + \frac{9(b_B^2 + a_B^2)}{(b-a)^2}}, \tag{2.16}$$

and for Ek,

$$\mathrm{Ek}_\sigma = \sqrt{\Omega_\sigma^2 + \frac{4(b_B^2 + a_B^2)}{(b-a)^2}}. \tag{2.17}$$

Standard Error	Equation Number	Experiment Series					
		4U-8L	8M-9L	126-166	167-227	228-254	255-281
a_σ %	2.5	0.16	0.16	0.16	0.16	0.16	0.16
b_σ %	2.5	0.13	0.13	0.13	0.13	0.13	0.13
d_σ %	2.5	0.36	0.36	0.38	0.38	0.37	0.37
Ω_σ %	§2.2.2	0.07	0.07	0.07	0.07	0.07	0.07
ΔT_B °C	2.6	0.013	0.057	0.0068	0.010	0.003	0.011
ΔT_σ %	2.7	0.33	0.57	0.17	0.10	0.08	0.11
H_B *watts*	2.8	0.22	0.22	0.18	0.16	0.078	0.24
H_σ %	2.9	1.3	0.41	1.3	0.31	0.58	0.49
$(H_{cond})_\sigma$ %	2.10	0.53	0.70	0.46	0.44	0.43	0.44
Nu_σ %	2.11	1.4	0.81	1.4	0.54	0.72	0.66
$[\mathrm{Nu}/\mathrm{Nu}(0)]_\sigma$ %	2.12	1.7	1.1	1.7	0.60	0.88	0.81
$(\Delta T_B)_B$ °C	2.13	0.014	0.014	0.0095	0.0049	0.040	0.060
$(\Delta T_B)_\sigma$ %	§2.2.7	2.5	1.4	1.1	1.0	17.0	15.0
Θ_σ %	2.14	0.51	0.69	0.44	0.42	0.40	0.41
τ_σ %	2.15	0.39	0.39	0.41	0.41	0.40	0.40
Ra_σ %	2.16	0.33	0.57	0.17	0.10	0.08	0.11
Ek_σ %	2.17	0.07	0.07	0.07	0.07	0.07	0.07
$(A_*^{-1})_\sigma$ %	2.18	5.8	5.3	1.8	1.2	-	-
$(H_\eta)_\sigma$ %	2.19	2.6	1.5	-	-	-	-

TABLE 2.2: Standard errors in the experimental control parameters, measurements and quantities derived from them.

The quantity A_*^{-1} is defined in equation (3.17), and so its error is

$$(A_*^{-1})_\sigma = \sqrt{\Omega_\sigma^2 + (H_{adv})_\sigma^2 + (\Delta T_B)_\sigma^2 + \Delta T_\sigma^2}. \tag{2.18}$$

$H_\eta(\bar{r}, a = 0; t)$ is given in equation (3.16), the error in H_η when $a \neq 0$ was assumed to be the same as when $a = 0$ providing that the average depth of the system $\bar{d}$ was used instead of d. Thus

$$(H_\eta)_\sigma \approx \sqrt{(\Delta T_B)_\sigma^2 + \Delta T_\sigma^2 + 2d_\sigma^2 + \Omega_\sigma^2}. \tag{2.19}$$

The error in H_ζ is discussed in §3.2.5 when that quantity is calculated. Here the error is simply stated as $(H_\zeta)_\sigma = 15\%$ at $\Delta T \approx 4\ K$, and $(H_\zeta)_\sigma = 17\%$ at

$\Delta T \approx 10\ K$.

These results were used to calculate the standard errors given in *Table 2.2.*

Standard Error	Equation Number	Experiment Series					
		282-309	310-336	337-364	365-391	012-021 042-046	022-041
a_σ %	2.5	0.16	0.16	0.16	0.16	0.16	0.16
b_σ %	2.5	0.13	0.13	0.13	0.13	0.13	0.13
d_σ %	2.5	0.46	0.46	0.46	0.46	0.36	0.36
Ω_σ %	§2.2.2	0.07	0.07	0.07	0.07	0.07	0.07
$\Delta T_B\ ^\circ C$	2.6	0.011	0.010	0.019	0.015	0.016	0.046
ΔT_σ %	2.7	0.28	0.10	0.48	0.15	0.39	0.46
$H_B\ watts$	2.8	0.30	0.30	0.40	0.64	0.22	0.22
H_σ %	2.9	2.3	0.68	3.6	1.6	1.3	0.41
$(H_{cond})_\sigma$ %	2.10	0.58	0.51	0.70	0.53	0.57	0.38
Nu_σ %	2.11	2.4	0.85	3.7	1.7	1.4	0.56
$[\mathrm{Nu}/\mathrm{Nu}(0)]_\sigma$ %	2.12	2.8	1.0	4.5	2.1	1.7	0.69
$(\Delta T_B)_B\ ^\circ C$	2.13	0.0080	0.016	0.016	0.016	0.011	0.012
$(\Delta T_B)_\sigma$ %	§2.2.7	0.84	0.83	1.3	0.66	1.7	0.94
Θ_σ %	2.14	0.56	0.49	0.68	0.50	0.55	0.60
τ_σ %	2.15	0.48	0.48	0.48	0.48	0.39	0.39
Ra_σ %	2.16	0.28	0.10	0.48	0.15	0.39	0.46
Ek_σ %	2.17	0.07	0.07	0.07	0.07	0.07	0.07
$(A_*^{-1})_\sigma$ %	2.18	2.5	1.3	3.9	1.9	2.2	1.2
$(H_\eta)_\sigma$ %	2.19	1.1	1.1	1.5	0.9	1.8	1.1

TABLE 2.2 (continued).